Gold-induced reconstructions of the Si(001) surface: The 5×3 and $\sqrt{26}\times3$ phases

X. F. Lin, K. J. Wan, J. C. Glueckstein, and J. Nogami*
Department of Physics and Laboratory for Surface Studies, University of Wisconsin-Milwaukee, Milwaukee, Wisconsin 53201
(Received 22 July 1992)

Scanning tunneling microscopy (STM) and low-energy electron diffraction have been used to study surface reconstructions of Au on the Si(001) surface. A previously reported $\sqrt{26}\times3$ superstructure diffraction pattern is shown to correspond to a mixture of 5×3 and $\sqrt{26}\times3$ phases with the structure of these two phases being closely related. In both structures, the spacing of the surface atoms in the STM images shows a strong uniaxial compression of 17% with respect to the bulk 1×1 lattice spacing.

Surface reconstructions of Au on the Si(001) surface have been studied by different techniques.[1-3] Systematic studies were done by Oura and Hanawa[2] using low-energy electron diffraction (LEED) and Auger electron spectroscopy to study the growth of Au on Si(001) as a function of both Au coverage and annealing temperature. Briefly, their studies show that when a small amount of Au is deposited onto the substrate at room temperature and then annealed up to about 400 °C, the (2×1) LEED pattern of the original surface degrades gradually with coverage, disappearing at about 0.5 monolayers (ML). With a further increase of Au deposition, there is evidence of reaction seen in the Si *LVV* Auger signal, along with diffraction features that indicate polycrystalline growth of either Au or a Au silicide. Heating up to several ML of Au above 400 °C produces a series of ordered superstructures. A $c(8\times2)$ structure is seen between 600 and 750 °C, which converts to $\sqrt{26}\times1$ at about 800 °C. Above 850 °C, a $\sqrt{26}\times3$ structure is observed. They suggest that the best Au coverages for the formation of these superstructures are 0.5 ML for $c(8\times2)$ and 1 ML for $\sqrt{26}\times3$. Using reflection electron microscopy, Yagi *et al.* have also observed the $\sqrt{26}\times3$ superstructure.[3]

We have used primarily scanning tunneling microscopy (STM) to study the behavior of the Au/Si(001) system for Au coverages up to 3 ML and the annealing temperatures between room temperature (RT) and 1000 °C. In particular, we have observed both the $c(8\times2)$ and the $\sqrt{26}\times3$ reconstructions at Au coverages and substrate annealing temperatures that are in agreement with previous work.[2] In this paper, we present our results on the $\sqrt{26}\times3$ phase. We have characterized this phase with LEED, STM, and x-ray photoelectron spectroscopy (XPS). The LEED results help to clarify the correspondence between the STM images and the previously reported diffraction studies. Preliminary XPS results allow us to place limits on the Au surface atomic density in the $\sqrt{26}\times3$ phase. Other aspects of the Au/Si(001) system will be discussed elsewhere.

All experiments were performed in an ultrahigh-vacuum chamber having a base pressure of less than 7×10^{-11} Torr. The chamber was equipped with a STM,[4] a four-grid LEED optics, and facilities for sample heating and metal deposition. The Si(001) samples were cut from silicon wafers, chemically cleaned immediately before introduction to the chamber, and then outgassed by heating to 700 °C at a pressure of less than 1×10^{-10} Torr. After outgassing, they were flashed briefly to 1150 °C to remove the surface oxide, cooled rapidly to 1000 °C and held there for 10 min, then cooled slowly to RT. All samples were characterized by both STM and LEED. Au was evaporated from a tungsten filament onto substrates at RT. The evaporation rate was calibrated versus evaporator filament power by a quartz-crystal-thickness monitor, and Au coverages were determined by timed exposure to the source. Samples were annealed after Au deposition. Substrate temperatures were measured by a calibrated thermocouple and an infrared pyrometer. All samples were allowed to cool to RT before either STM or LEED measurements were taken. The XPS measurements were taken in a separate chamber with samples prepared *in situ* under similar conditions.

Both our LEED and STM measurements indicate that the previously reported $\sqrt{26}\times3$ phase corresponds to a mixture of 5×3 and $\sqrt{26}\times3$ surface structures. These two phases coexist on the surface over the Au coverage range 0.6–3 ML at annealing temperatures of 760–850 °C. These parameters fall within the ranges indicated in previous work for producing the $\sqrt{26}\times1$ and $\sqrt{26}\times3$ phases.[2] There was a slight dependence of the annealing temperature with Au coverage for the sharpest LEED patterns. Higher annealing temperatures were necessary for specimens with more deposited Au. Purely 5×3 or $\sqrt{26}\times3$ ordering was never observed.

A STM topograph of a typical area of the mixed $5\times3/\sqrt{26}\times3$ reconstruction (hereafter this mixed phase is denoted $\sqrt{26}$) is shown in Fig. 1. This image was taken tunneling from the filled states with a sample bias voltage of -1.5 V and a tunneling current of 0.8 nA. The topograph consists of stripes running along $\langle 1\bar{1}0\rangle$ directions with a perpendicular spacing of $5a$ (where $a=a_0/\sqrt{2}=3.84$ Å). The basic structure within each stripe is four parallel rows of atomic scale features of two different sizes with a lower density of very prominent bright features on some of the stripes. The stripes are separated by trenches. We will refer to the stripes without the large bright features as type (i) and those with the large bright features as type (ii). Figure 2 is a schematic of the features seen in Fig. 1. (The orientation

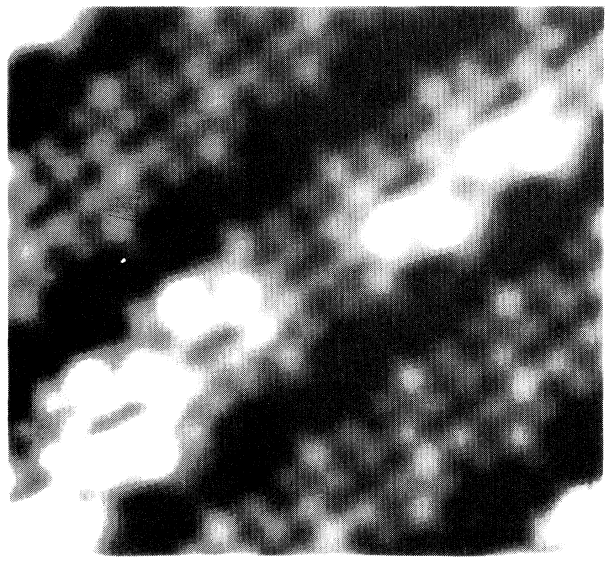

FIG. 1. A 50×50 Å filled state image of the mixed $5\times3/\sqrt{26}\times3$ phase.

of the samples in the STM with respect to the scanning direction is such that $\langle 1\bar{1}0\rangle$ directions are oriented at $\approx 45°$ from the horizontal in all of the images in this paper. For simplicity, schematics such as Fig. 2 have $\langle 1\bar{1}0\rangle$ directions either horizontal or vertical.) The three types of atomic features are labeled *A*, *B*, and *C*, in order of increasing size. There are also atomic scale features visible on the bottom of each trench. However, the registration between the features on the stripes and in the trenches varies with bias voltage so we will only consider the structure on the stripes in our analysis.

We discuss first the structure of the type-(i) stripes without the larger type-*C* features. Each stripe has four rows of features which are spaced at distances of 1*a* along the stripe direction, with periodic switching between type-*A* and -*B* features resulting in a pattern with 3*a* periodicity. Adjacent type-(i) stripes give rise to rows of 5×3 unit cells. Although the structure within each stripe is approximately a square 1×1 lattice, the spacing of the atomic scale features can be smaller perpendicular to the stripe direction than the spacing along the stripe. This is clearer in Fig. 2 where half of the diagram shows a superimposed square array of black dots at a 1×1 unit-cell spacing. Within each stripe, the two central rows are about 1*a* apart, whereas the outer rows are displaced towards the center of the stripe. This uniaxial compression of the surface atomic features will be discussed in more detail later.

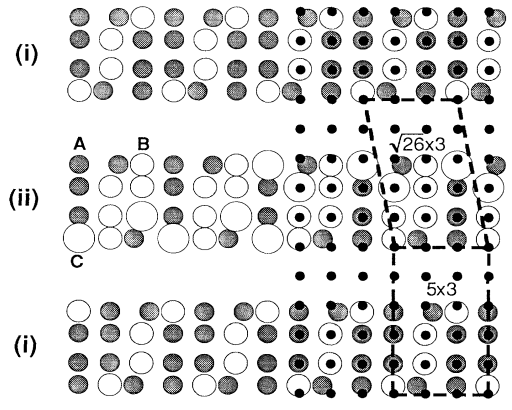

FIG. 2. A diagram of the image in Fig. 1, showing type-(i) and -(ii) stripes, and a phase slip between two type-(i) stripes. Both $\sqrt{26}\times3$ and 5×3 unit cells are outlined. Half of the figure has a superimposed grid of 1×1 atomic positions marked by black circles.

Now we consider the structure of the type-(ii) stripes that contain a series of type-*C* features along their length. Although the structure of these stripes is dominated by the bright type-*C* features, the areas adjacent to these features are similar to the type-(i) stripes, with four rows of approximately "1×1" unit-cell-spaced features having an analogous pattern of type-*A* and -*B* features with a 3*a* periodicity along the stripes. The type-*C* features are in registry with the 1×1 lattice defined by the smaller atomic features and always occur in diagonally spaced pairs. These pairs lie over pairs of rows that are adjacent to a trench, and never over the central pair of rows. The pairs are spaced 3*a* apart, except in those instances where the pairs switch from one side of a stripe to the other. Because the features in each pair are diagonally spaced, the pair is not symmetric in the mirror plane perpendicular to the stripe direction. There is also a specific relationship between the orientation of the pairs, and the background pattern of the type-*A* and -*B* features. In the background pattern visible in the type-(i) stripes, the brighter type-*B* features are in groups of four in a crooked line running diagonally across the stripe. A line drawn between the type-*C* features in any pair always runs across the direction of the diagonal lines of type-*B* features.

There is a crucial difference between the type-(i) and -(ii) stripes that influences the long-range order of the surface. This is most easily seen by examining Fig. 2 in conjunction with Fig. 1. Both types of stripes have a 3*a* periodicity along their length. However, this 3*a* periodicity is not necessarily in phase between different stripes. Adjacent type-(i) stripes remain in phase to produce 5×3 order. However, when there is a type-(ii) stripe between two type-(i) stripes, then there is a phase slip of 1*a* along the stripe direction of one type-(i) stripe with respect to the other. This phase slip produces $\sqrt{26}\times3$ order. In reference to Fig. 2, which shows a type-(ii) row between two type-(i) rows, the "upper" row is shifted 1*a* to the left with respect to the "lower" row. The area between all three stripes is then a combination of 5×3 unit cells and $\sqrt{26}\times3$ unit cells. Figure 2 also shows the particular relationship between the direction of the phase slip and the orientation of the diagonal type-*C* pairs which produces a particular orientation of the $\sqrt{26}\times3$ unit cells. In general, all four possible domains of the $\sqrt{26}\times3$ are observed on any given sample.

Thus, a surface covered in a mixture of type-(i) and -(ii)

stripes is covered in a mixture of 5×3 and $\sqrt{26}\times3$ unit cells. In essence, the bright type-C features mark lines of dislocations that disrupt what would otherwise be perfect 5×3 ordering. Figure 3 is a larger area scan of the $\sqrt{26}$ surface on a different sample. From this image, it is clear that lines of type-C features are connected on a longer scale, even as they skip from stripe to stripe. The average spacing between the dislocations measured in the direction perpendicular to the stripes is about two stripe widths. This implies that there is an equal population of 5×3 and $\sqrt{26}\times3$ unit cells on the surface. We have found that the density of type-C features, and hence the relative populations of the 5×3 and the $\sqrt{26}\times3$ phases, is the same for all the $\sqrt{26}$ surfaces that we have prepared over the whole range of Au coverages and annealing temperatures for the formation of this $5\times3/\sqrt{26}\times3$ mixed phase.

We now examine the bias dependence of the images more closely. Figure 4 shows a dual-bias image of the $\sqrt{26}$ surface. This pair of images was taken tunneling into and out of the same sample area with sample bias voltages of -0.9 V and $+0.9$ V, thus reflecting (a) filled and (b) empty states of the sample, respectively.

The overall appearance of the structure is similar at either bias polarity, with stripes, each made up of four rows of atomic features, well separated by trenches. The most striking difference between the two images is that the type-C features that are so prominent in the filled states are no more prominent than the other atomic features in the empty states. The only exception to this behavior occurs where there is a higher local density of type-C features, such as when these features switch between the two sides of a stripe, or when there are type-C features on the rows immediately adjacent to both sides of a trench (this second configuration is not seen in Fig. 4). In these areas, there is a higher density of empty states which makes several of the atomic features brighter.

Figures 5(a) and 5(b) are diagrams of the positions of the bright features seen in both bias polarities in Fig. 4.

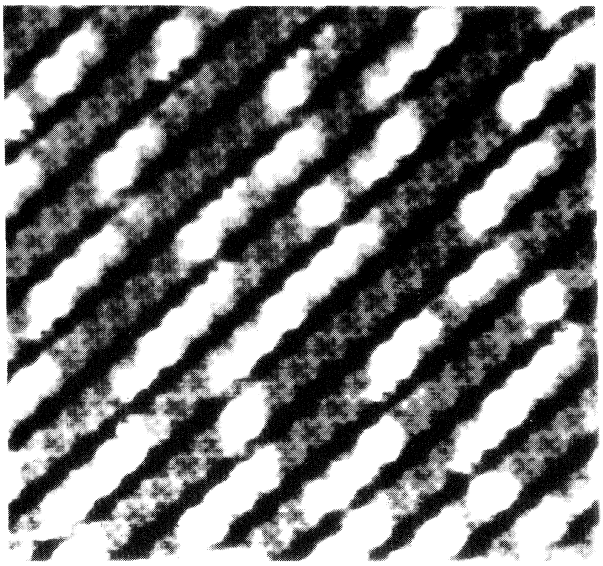

FIG. 3. A 200×200 Å filled state image of the $\sqrt{26}$ phase.

The filled states shown in Fig. 5(a) show a different orientation of the $\sqrt{26}\times3$ structure from that in Fig. 2, just as in the corresponding images [Fig. 4(a) versus Fig. 1]. The two different domains are related by a mirror reflection in the plane perpendicular to the stripe direction. Ignoring the presence of the previously discussed type-C features, the principal features of the filled states are stripes with four rows of atomic scale features in an approximately 1×1 square lattice, and a periodic spacing of brighter features defining a $3a$ periodicity along the rows. The spacing of the rows of atomic features is also uneven across the stripe, with the central pair being slightly farther apart than the pair of rows adjacent to the trench on either side, as was already mentioned.

The empty state features are similar to the filled states, but they differ in several respects. First, as was already

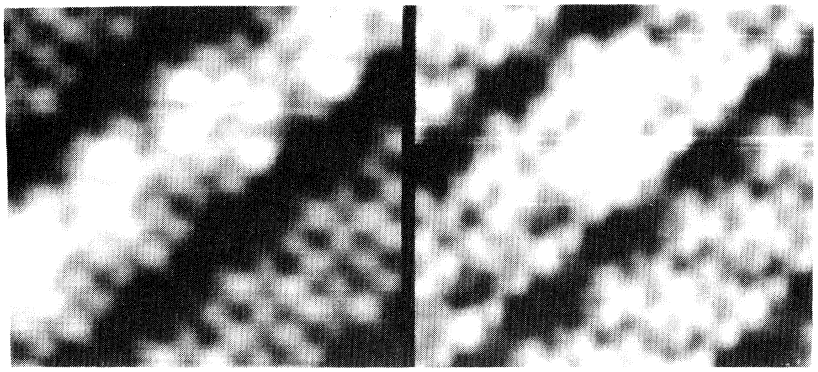

FIG. 4. Dual-bias images of the $\sqrt{26}$ phase, showing the (a) filled and (b) empty states of the same area.

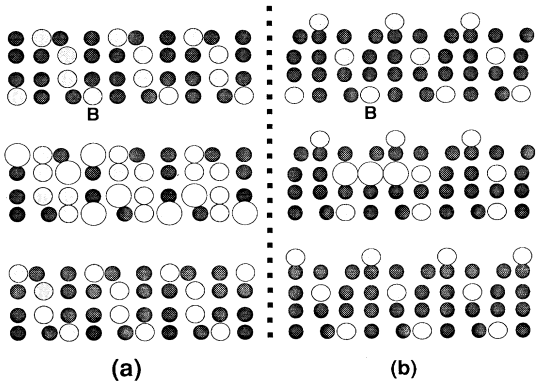

FIG. 5. A schematic of the images in Fig. 4 with (a) being the filled and (b) empty states. The features marked "*B*" in both panels are in the same physical location.

mentioned, type-*C* features so prominent in the filled states are approximately the same height as the rest of the features on the stripes. There is a similar pattern of brighter features that define the $3a$ periodicity, but with triplets of atomic scale features, rather than groups of four. These brighter features are in phase with the brighter ones in the filled states: the positions marked "*B*" in both panels of Fig. 5 are in registry. More generally, the "1×1" square lattices seen in both biases are in phase. The relative spacing of the atomic features in the approximately 1×1 lattices differ slightly in the two images. For the empty states, the distance between the central pair of rows is slightly smaller than that between the outermost rows and their neighbors. This is opposite to the spacing in the filled states. There is also a clear asymmetry across each stripe in the empty states, with a row of protruding features extending from one edge of the stripe. These protrusions are reproducible for different samples and different tips, and so it would appear that there is a genuine asymmetry in these stripes. However, this asymmetry would have to be subtle since it is not apparent in the filled states images. The protrusions might be due to differences in the bonding arrangement of the atoms on the edges of the stripes with the layer below that forms the floor of the trenches.

In view of the similarity between both filled and empty state images, it is reasonable to suggest that the basic structure of the stripes is a 1×1 lattice of surface atoms, either Au or Si, with slight pairwise interactions and buckling causing small periodic variations in both the height and the spacing of these features. These variations are also visible as patterns of slightly wider spacings between atoms that form dark diagonal lines across the stripes in the empty states, and a more symmetric cross hatched pattern in the filled states. The relative prominence of the type-*C* features in the filled states is due to the effects of electronic structure since these features are not particularly distinguishable from their neighbors in the empty states.

Now we return to the question of the uniaxial compression of the atomic features within each stripe. This compression cannot be accurately evaluated from an image of a single domain of the $\sqrt{26}$ structure since any STM image has a linear distortion that is usually due to thermal drift during the acquisition of the image. This drift is corrected by applying an appropriate linear mapping that restores the correct aspect ratio and geometry of the structures in the image. For structures of unknown geometry, this correction process has undetermined parameters. However, if one can obtain an image at a step edge on the Si(001) surface, then the surface geometry can be determined uniquely. Figure 6 shows an image of two domains of the $\sqrt{26}$ structure bordering a step edge, which rotates the structure on one terrace by 90°. This image has been corrected so that the unit cells in both domains have the same aspect ratio. By this means, it was possible to determine that 5×3 was indeed the correct periodicity of the surface structure.

Using this corrected image, we can evaluate the uniaxial distortion reliably. Two white lines, a distance $3a$ apart, have been drawn perpendicular to the stripes on the higher terrace, extending over the lower terrace. This is also illustrated in Fig. 7. These lines clearly lie outside the centers of the outermost rows in a stripe on the lower terrace. Since the width of the stripe comprises four atomic scale features, this means that the average distance between the features across the stripe is smaller than that along the stripe.

We have measured the compression by drawing lines through the average positions of the centers of the outermost rows in several adjacent stripes (as shown in Fig. 7), and then comparing the ratio of the distances across a stripe ("*M*"), and between two stripes ("*N*"). If the atom-

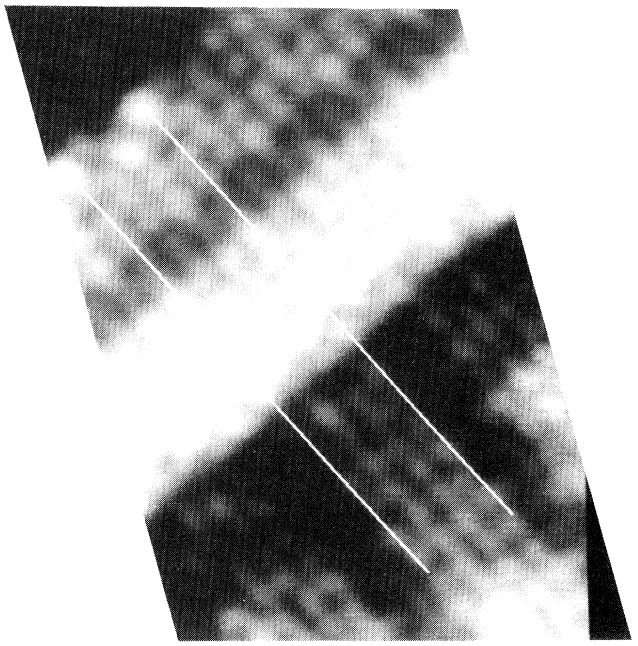

FIG. 6. A filled state image of two domains of the $\sqrt{26}$ phase bordering both sides of a single height atomic step. Two parallel white lines drawn $3a$ apart extend from the upper to the lower terrace.

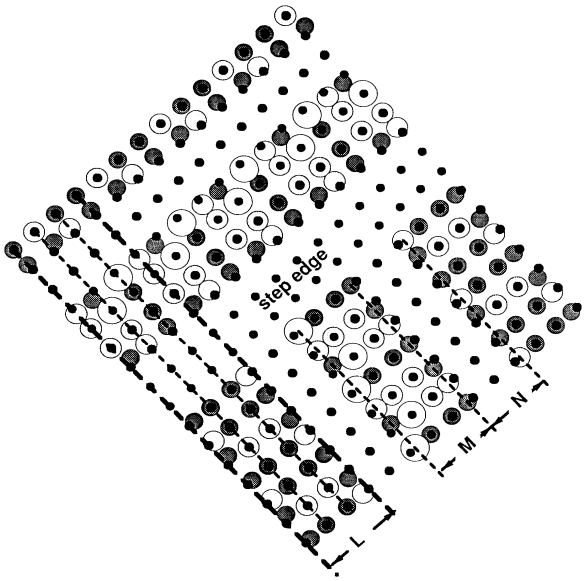

FIG. 7. A diagram of the image in Fig. 6 (see text for details).

ic features are on a uniform 1×1 grid, then this ratio should be $\frac{3}{2}$. The actual value is 1.0 which means that the average spacing of the four atomic features across the stripe is 0.83 times the spacing along the stripe. Thus there is a compression of about 17% across each stripe. A 1×1 grid of black dots has been drawn in both Fig. 7 and in part of Fig. 2 to illustrate the compression.

The uniaxial nature of the compression suggests that the surface atoms have an anisotropic bonding environment. One possibility is that the surface is similar to an unreconstructed Si(001) surface with all surface atoms having twofold coordination with the underlying atoms. This arrangement allows the atomic positions to move much more easily in the direction perpendicular to rather than parallel to the subsurface neighbors. This behavior is somewhat analogous to the dimerization of the clean Si(001) surface.

Adsorbate-induced expansion or compression of a 1×1 surface atomic lattice has been seen for several metals on Si(111).[5,6] However, in these cases the strain is isotropic because of the symmetry of the surface. This strain is relieved by the periodic interruptions of the 1×1 structure, resulting in an extended superlattice periodicity which can be either commensurate or incommensurate with the substrate lattice.

Figures 8 and 9 show a LEED pattern of the mixed $\sqrt{26}$ phase and a diagram of all superstructure dots corresponding to the 5×3 and the $\sqrt{26}\times3$ periodicities. This particular surface was prepared by annealing 0.8 ML of Au at 800 °C. This LEED pattern taken at 55 eV shows a mixture of two domains of 5×3 structure and four domains of $\sqrt{26}\times3$ structure. The dots that are prominent in the LEED pattern are indicated by circles in Fig. 8. The relative intensities of the dots are a function of the beam energy, but some features of both the 5×3 and the $\sqrt{26}\times3$ periodicities are visible at all energies.

As to why an earlier LEED study[1] identified both a $\sqrt{26}\times1$ and a $\sqrt{26}\times3$ phase, we note that $\sqrt{26}\times1$ structure reflections are in the same positions as those for a 5×1 structure, and that the $\sqrt{26}\times1$ structure was also reported to have weak $\frac{1}{3}$ order streaks. Thus we believe that the $\sqrt{26}\times1$ pattern corresponds to a slightly disordered 5×3 pattern. The earlier study also reported that $\sqrt{26}\times1$ and $\sqrt{26}\times3$ phases were very close together in the phase diagram, which is also consistent with our observation of a mixture of two phases in a similar range of coverages and annealing temperatures.

The STM gives us an opportunity to see the real space of the surface. With the help of other surface study techniques, we can get other information about the surface such as the surface atomic composition. Following the STM and LEED work, we used x-ray photoelectron spectroscopy to investigate the surface atomic composition

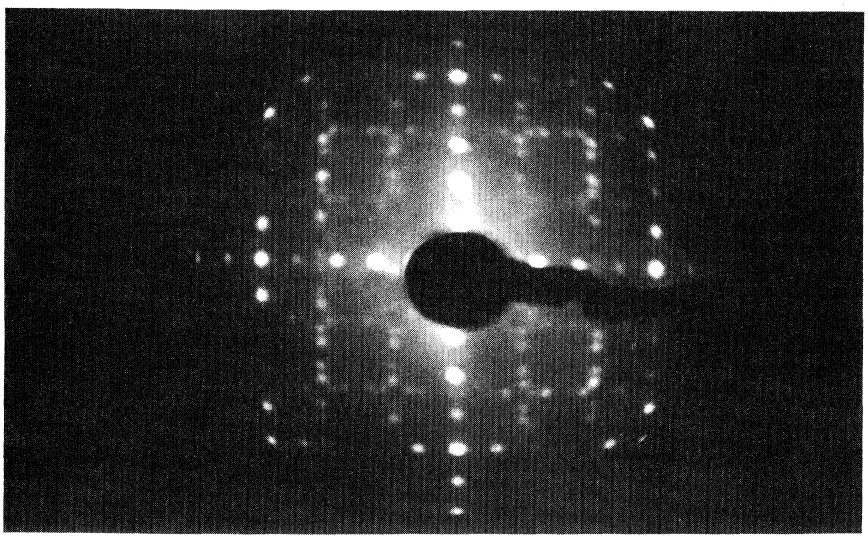

FIG. 8. A LEED pattern of the mixed phase surface at a beam energy of 55 eV.

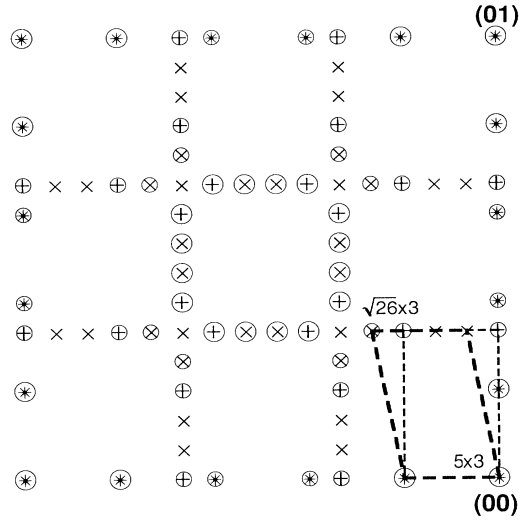

FIG. 9. Schematic of the LEED pattern in Fig. 8, showing all possible domains of the 5×3 and the $\sqrt{26}\times3$ phases. 5×3 spots are marked with $+$, $\sqrt{26}\times3$ spots with $\times$, and spots common to both with $\otimes$. Spots visible in the LEED pattern are circled, with two sizes of circles indicating relative intensities.

for the different Au/Si(001) surface structures. Similar XPS studies of Au on Si(001) are found in Refs. 7 and 8, although not specifically for the Au/Si(001) superstructures that we examine here. All XPS measurements were carried out with a VG ESCALAB system equipped with dual anodes, a hemispherical analyzer, LEED optics, and facilities for sample heating and metal deposition. The sample preparation was the same as for the STM experiments. X-ray radiation was provided by the Al κ_α line at 1486.6 eV. During both sample preparation and measurement, the analysis chamber and any materials therein were maintained at a pressure $<1\times10^{-9}$ Torr. Each sample was first characterized by LEED to check for the appropriate superstructure. The peak areas of core-level states for Au $4f_{7/2}$ and Si $2p$ were measured as quantitative data and were used in the calculation of the surface atomic composition, with the assumption that the surface atomic sensitivities are the same as the known values in the bulk. Spectra were also taken at different take-off angles to vary the surface sensitivity of the measurements.

Our STM studies of Au growth on Si(001) at RT show that all of the deposited Au remains on the surface for coverages up to 1.3 ML. This provides us with a known configuration when we compare the Au/Si ratio for a given coverage at RT and after annealing. For up to 1.2 ML of Au, annealing the sample at temperatures above 500 °C strongly decreases the Au/Si ratio. Analysis of the changes in the Au/Si XPS ratios shows that after annealing, there are some Au atoms which still reside within the top few layers of Si atoms, with the remaining Au diffusing into the bulk out of range of the XPS measurement, or leaving the surface altogether. The Au atoms which remain at or near the surface presumably are responsible for forming the superstructures. With increasing annealing temperatures up to 1000 °C, more and more Au atoms leave the near-surface region. For example, when 1.2 ML of Au is deposited onto the substrate at RT and then annealed at 800 °C, the surface shows $5\times3+\sqrt{26}\times3$ structure in the LEED pattern, and the ratio of Au $4f_{7/2}$ to Si $2p$ measured at normal emission is decreased from 1.2 at RT to 0.7 after annealing. Quantitative modeling shows that this decrease in the Au/Si ratio is consistent with a total of 0.6 ML Au residing in the first two atomic layers, and the remaining Au diffusing deep into the bulk. This implies that the maximum possible surface concentration of Au on the surface is 0.6 ML for the $5\times3+\sqrt{26}\times3$ mixed phase. It is also possible that the Au is distributed in the first three or four atomic layers in which case the surface concentration of Au would be still lower. In any case, this means that all of the atomic scale features of $\sqrt{26}$ phase in the STM images cannot be due to Au atoms. There is not enough information in the XPS data to make a more accurate estimate of the Au surface atomic density and so it is not possible to assign specific types of surface features in the STM images to either Au or Si atoms.

In conclusion, we have studied Au-induced reconstructions of the Si(001) surface that have been described as $\sqrt{26}\times3$ and $\sqrt{26}\times1$ superstructures in previous studies. Our STM measurements show that the surface is actually a mixture of 5×3 and $\sqrt{26}\times3$ ordered phases. These two phases are closely related, with the basic structure for both being a series of stripes running along $\langle 1\bar{1}0\rangle$ directions with each stripe having a raised portion with four rows of an approximately 1×1 atomic lattice and an adjacent trench. The positions and intensities of the atomic features are modulated to produce a three unit-cell periodicity along each stripe. In addition, there is a uniaxial compression of the 1×1 atomic positions perpendicular to the stripe. XPS measurements indicate that less than 60% of the atomic features seen in the STM images are due to Au atoms.

We acknowledge the help of Steve Hardcastle during the XPS measurements.

*Author to whom all correspondence should be sent.

[1]Kenjiro Oura, Yoshikazu Makino, and Teruo Hanawa, Jpn. J. Appl. Phys. **15**, 737 (1976).

[2]Kenjiro Oura and Teruo Hanawa, Surf. Sci. **82**, 202 (1979).

[3]K. Yagi, N. Osakabe, Y. Tanishiro, and G. Honjo, in *Proceedings of the Fourth International Conference on Solid Surfaces, Cannes 1980,* edited by D. A. Degros and M. Costa (Le Vide, Les Couches Minces, 1980), Vol. 210, p. 1007.

[4]Commercial STM by Omicron GmbH, Taunusstein, FRG.

[5]D. M. Chen, J. A. Golovchenko, P. Bedrossian, and K. Mortensen, Phys. Rev. Lett. **61**, 2867 (1988).

[6]R. J. Wilson, S. Chiang, and F. Salvan, Phys. Rev. B **38**, 12 696 (1988).

[7]K. Hricovini, J. E. Bonnet, B. Carrière, J. P. Deville, M. Hanbücken, and G. LeLay, Surf. Sci. **211/212**, 630 (1989).

[8]Z. H. Lu, T. K. Sham, K. Griffiths, and P. R. Norton, Solid State Commun. **76**, 113, (1990).

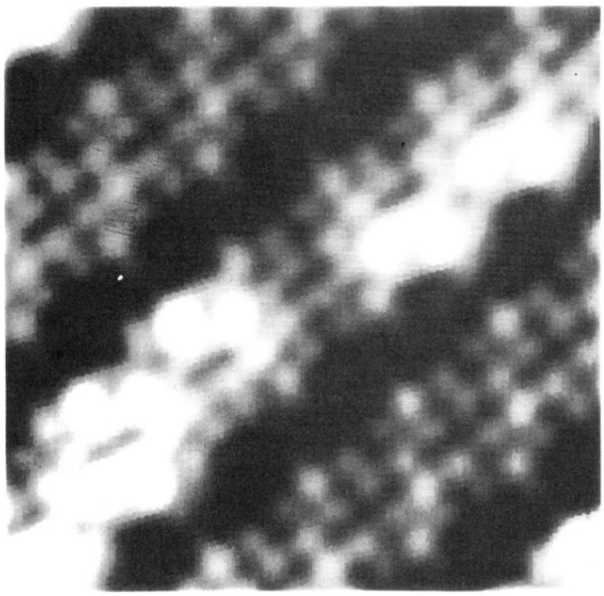

FIG. 1. A 50×50 Å filled state image of the mixed $5 \times 3/\sqrt{26} \times 3$ phase.

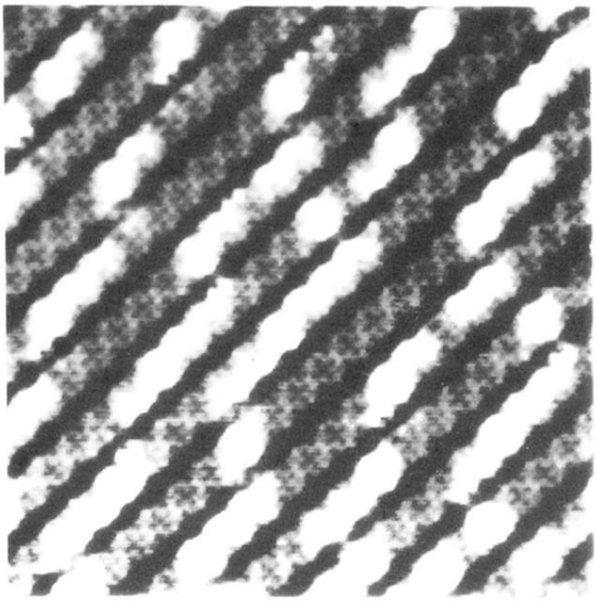

FIG. 3. A 200×200 Å filled state image of the $\sqrt{26}$ phase.

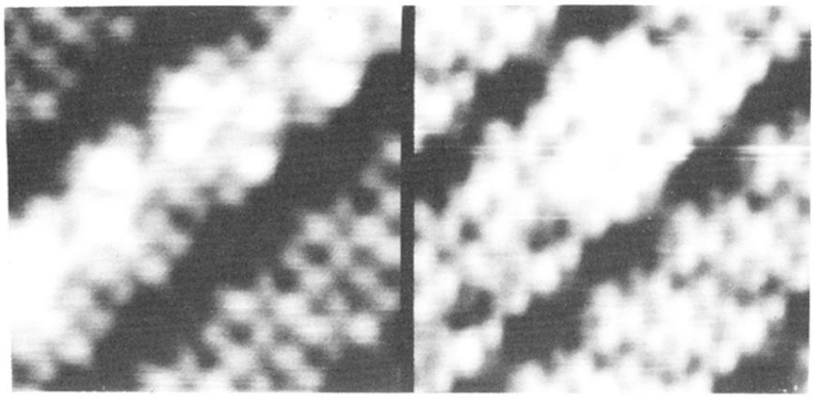

FIG. 4. Dual-bias images of the $\sqrt{26}$ phase, showing the (a) filled and (b) empty states of the same area.

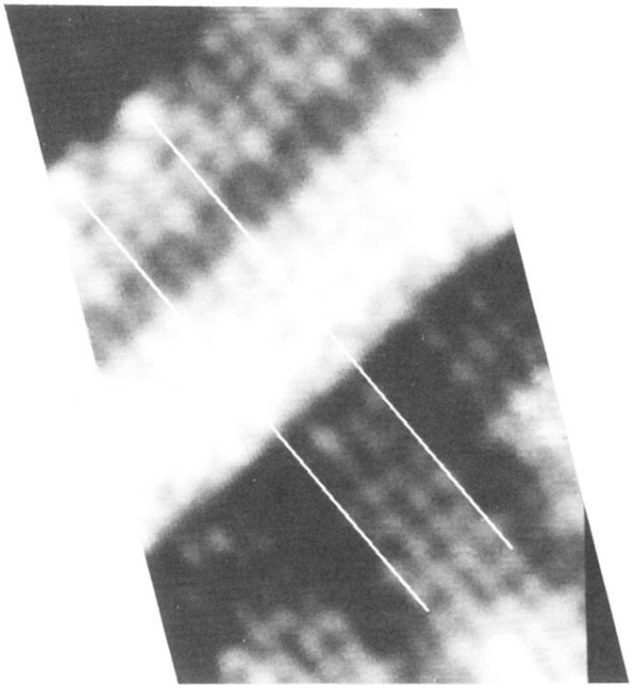

FIG. 6. A filled state image of two domains of the $\sqrt{26}$ phase bordering both sides of a single height atomic step. Two parallel white lines drawn $3a$ apart extend from the upper to the lower terrace.

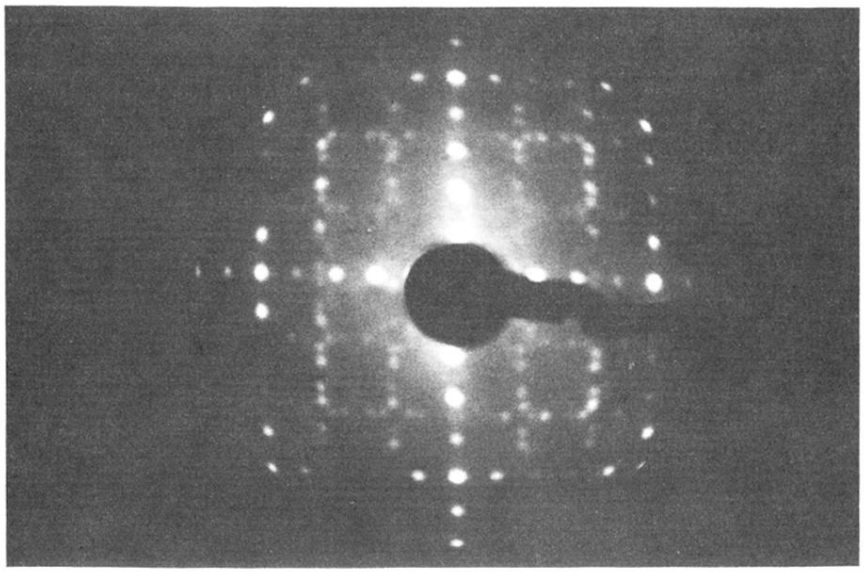

FIG. 8. A LEED pattern of the mixed phase surface at a beam energy of 55 eV.